Design of a Mechanism for Biaxial Rotation of a Wing for a Hovering Vehicle

Sean H. McIntosh, *Fellow, IEEE*, Sunil K. Agrawal, *Member, IEEE*, and Zaeem Khan

***Abstract*—This paper presents a novel mechanism to actuate the wings of a hovering micro air vehicle (MAV). The mechanism uses a single actuator, but each wing can rotate about two orthogonal axes. The goal of this work is to design a light-weight compact mechanism that flaps the wings, inspired from the wing motion of hummingbird and hovering insects, to generate enough lift for the vehicle to hover. This paper explains in detail the proposed mechanism and its working prototypes. Also, the paper presents a dynamic simulation of the mechanism. The proposed dynamic simulation is used to predict the theoretical lift of the ornithopter. Further, the theoretical model is supported by actual experimental data collected from the prototype. The experimental data shows that the vehicle has the potential to develop enough lift to hover.**

***Index Terms*—Flapping wing flight, hovering, micro air vehicles (MAVs), ornithopter.**

NOMENCLATURE

M_θ	Moment generated by the bending spring.
M_ψ	External moment in the ψ direction.
M_ϕ	Moment generated by torsion spring.
k_θ	Stiffness of the bending spring.
k_ϕ	Stiffness of the torsion spring.
E	Reference frame attached to the body.
F	Reference frame attached to the wing.
$x_\mathrm{o}, y_\mathrm{o}, z_\mathrm{o}$	Axes attached to the body.
$x_\mathrm{w}, y_\mathrm{w}, z_\mathrm{w}$	Axes attached to the wing.
x_1, y_1, z_1	Point on wingspar attached to the follower.
x_2, y_2, z_2	End point of the follower.
α	Angular acceleration of the wing.
ω	Anglular velocity of the wing.
θ	Wing rotation angle about the z_w axis.
ψ	Wing rotation angle about the x_w axis.
ϕ	Wing rotation angle about the y_w axis.
I	Moment of inertia of the wing.
m	Slope of guide.
F_x, F_y, F_z	Reaction force of wing support.
N_guide	Normal force exerted by the guide.
l_follower	Length of the follower.
l_rod	Length of wingspar from point o to the wing spar end of the follower.

Manuscript received September 15, 2005; revised November 30, 2005. Recommended by Guest Editor V. Krovi. This work was supported in part by the Army Research Office under Grant W911NF-05-1-0066.

The authors are with the University of Delaware, Newark, DE 19711 USA (e-mail: SHMcIntosh@gmail.com; agrawal@me.udel.edu; zakhan@me.udel.edu).

Digital Object Identifier 10.1109/TMECH.2006.871089

I. INTRODUCTION

In recent years, there has been a demand to reduce the size of unmanned air vehicles. The Defense Advanced Research Projects Agency (DARPA) defines the class of air vehicles measuring 15 cm or less in any dimension as micro air vehicles (MAVs). Possible applications of these vehicles range from civilian and military surveillance to search and rescue operations. Numerous research groups are actively developing designs of new MAVs. Some examples of MAVs are the *Black Widow*, developed by AeroVironment, Inc. [1], and the University of Florida's flexible wing design [2]. These MAVs, like the majority of MAVs, are scaled down versions of larger traditional flying vehicles, i.e., vehicles with fixed or rotary wings. Unfortunately, the Reynold's number and the aerodynamic lift of traditional flying vehicles decrease substantially as the wing length of the vehicles decrease [3].

Numerous research groups are attempting to solve the problem of low aerodynamic lift in MAVs by developing a class of MAVs known as ornithopters or flapping wing vehicles [4], [5]. The flapping wings of animals, and potentially the new flapping wing MAVs, rely on the translational motion, called the flapping, and the rotational motion, called the feathering, of their wings to develop unusually high lift. Experimental data has shown that the precise coordination of the flapping and feathering motions develops a number of beneficial aerodynamic mechanisms [3]. Some of the mechanisms to generate these additional lift, that have been recently studied by the biologists, include leading edge vortices, clap and fling, wake capture, virtual mass, and rotational forces [6], [7]. It is because of these studies, our group is attempting to create an ornithopter mimicking some of the basic insect wing motions to make use of these aerodynamic mechanisms to improve the flying capabilities.

At the University of Delaware, our group is actively pursuing new designs of flapping wing vehicles and studying their ability to fly [8]–[10]. The design considerations for these ornithopters consist of 1) an aerodynamically advantageous wing motion; 2) a light-weight and compact mechanism design; 3) a minimum number of actuators. Our earlier work was focused on forward-flying ornithopters with wing rotations about a single axis, found in large birds. The most effective of these designs was *Sparrow II* [11], which had flight durations of over a minute. Fig. 1(a) shows a picture of Sparrow II. In an attempt to mimic the wing motion of smaller birds and insects, our group is currently studying designs of ornithopters, which can rotate the wings about two orthogonal axes. The first attempt to design such a mechanism for the wings of an ornithopter is shown in Fig. 1(b) [10].

A number of useful lessons learnt from these early prototypes are incorporated into the ornithopter design described in this

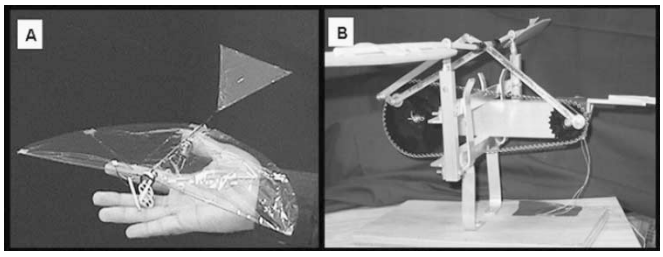

Fig. 1. (a) Photograph of *Sparrow II*, a successful forward flying ornithopter developed at the University of Delaware [11]. (b) Photograph of an ornithopter wing design at the University of Delaware with biaxial rotation [10].

Fig. 2. AutoCAD illustration of the flapping wing micro air vehicle described in this paper, which is capable of achieving biaxial rotation of the wings using only a single electric motor.

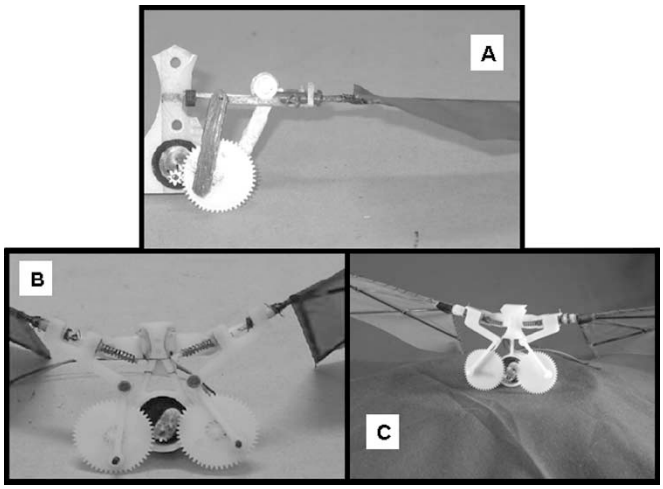

Fig. 3. A, B, and C show the iterations of the Mechanical Hummingbird Project, MHP I, MHP II, and MHP III, respectively.

paper. A CAD model of this design is shown in Fig. 2. This paper describes this ornithopter design, the mechanism it uses to create biaxial rotation of the wing using only a single actuator, a theoretical model to predict its dynamics and aerodynamics, and comparison of these results with experimentally collected wing force-torque data.

II. Novel Ornithopter Design

Our research work to create an ornithopter with biaxial wing rotation is named as the *Mechanical Hummingbird Project*—with the individual prototypes named *MHP I, MHP II*, and *MHP III*. Photographs of these three prototypes are shown in Fig. 3. Extensive experimental data has only been collected for

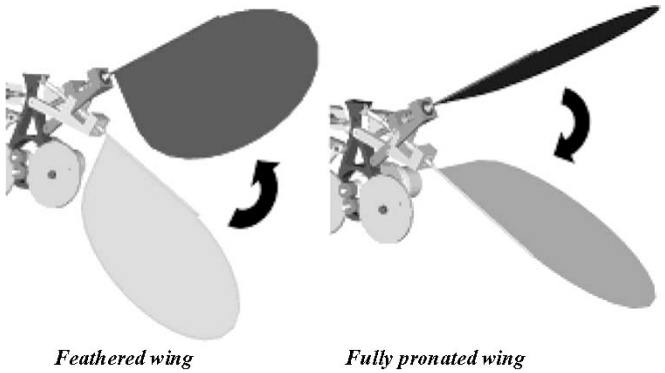

Fig. 4. Motion of the wing during the upstroke while it is feathered and during the downstroke when it is fully pronated.

MHP II and MHP III, and therefore, these are the focus in this paper. MHP II has a wingspan of 60 cm and a weight of 40 g. MHP III has a wingspan of only 48 cm with a weight of 50 g. (the extra weight is due to added sensors on the machine). These dimensions are slightly larger than the DARPA maximum but the goal is to shrink the size further over time.

The novel and unique features of this design are 1) a flapping mechanism that creates wing rotation about two orthogonal axes and 2) the two rotations of both wings are created using a single actuator. The mechanism creates a motion similar to insects and hummingbirds by quickly rotating the wing at the top and bottom of the up and downstroke. While the wing is translating downwards during flapping, the wing's flat surface is perpendicular to the direction of the wing motion, pulling the air along with it generating positive lift. At the bottom of the stroke, the wing quickly rotates or feathers, by approximately 45° about an axis through the wing spar. During the upstroke, the wing generates a negative lift. Since the wing has feathered, its effective surface area is reduced. Consequently, the magnitude of the negative lift during the upstroke is less than the positive lift generated during the downstroke. As a result, a net positive lift is generated. At the top of the stroke, the wing quickly rotates to its initial position and the process repeats during the next cycle. Fig. 4 illustrates this motion.

The mechanism consists of a body, a motor, two gear wheels, two connecting rods, two wing carriers, two wing spars with a wing, and a follower attached to opposite ends. Two guides are fixed to the body with the two torsion springs and two bending springs. In reality, these springs are compression springs but they are used in bending so the more descriptive term is used. Figs. 5–7 show schematics of the flapping mechanism and its different views for clarity.

The wing carrier supports the wing spar and attaches to the body by a pin joint. The wing spar rotates freely within the housing of the wing carrier but stops prevent it from sliding laterally. The connecting rod attaches to the wing carrier and a gear wheel by two pin joints at opposite ends. The gear wheels are pinned to the body. While the motor drives the right gear wheel directly, it indirectly drives the left gear through an idler gear. This system ensures symmetric flapping of the wings by rotating the gear wheels in opposite directions.

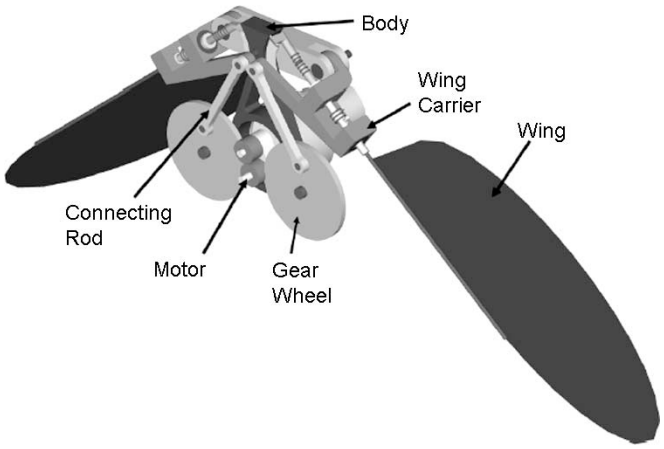

Fig. 5. Labeled three quarters view of the vehicle. The wings are rotated down and the follower rotated upward just above the guide.

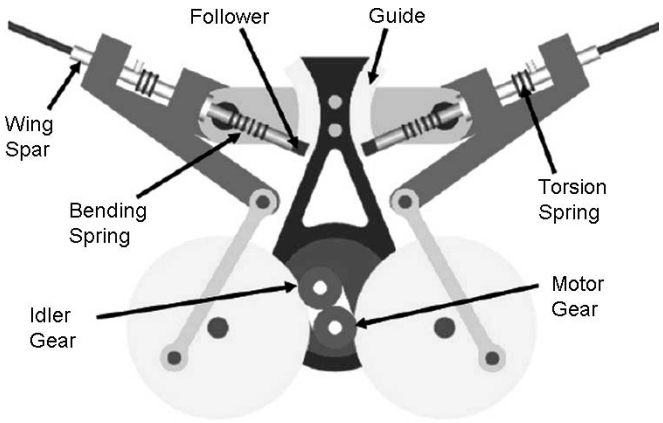

Fig. 6. Front view of the vehicle. This view shows the four-bar mechanism that drives the wings. Notice, how the motor gear drives the right gear wheel and idler gear.

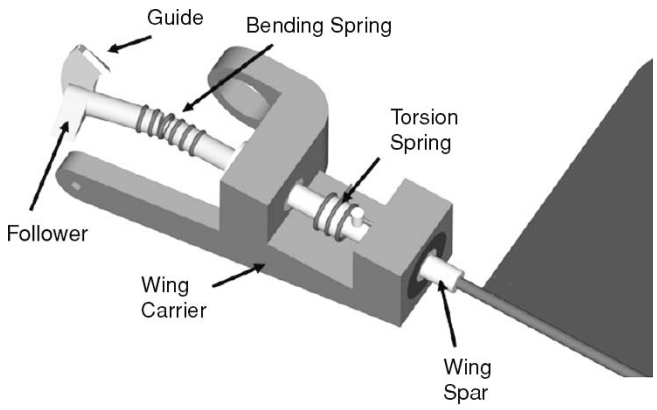

Fig. 7. Details of wing carrier assembly. The wing spar passes through the wing carrier and the torsion spring attaches to the wing spar. Also, the bending spring has deformed to allow the follower to move along the guide.

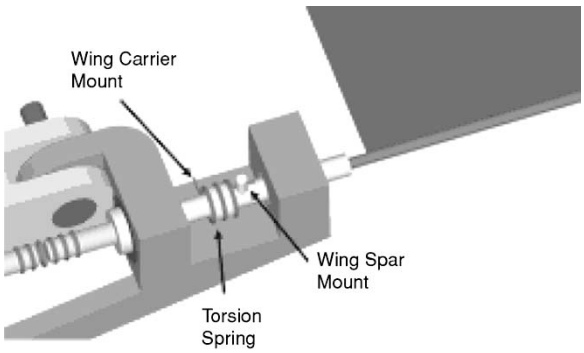

Fig. 8. Details of the torsion spring. The torsion spring attaches to the wing spar mount at one end and the wing carrier at the other. The spring creates a moment that acts to return the wing to its fully pronated position.

The wing spar assembly has three degrees-of-freedom: rotation about the pin joint that connects the wing carrier to the body (flapping axis), rotation about the axis of the wing spar (feathering axis), and deflection of the bending spring moving the follower out of alignment with the wing spar. The bending spring acts as a coupler connecting the follower to the wing spar. The bending spring creates a rigid connection in torsion but allows for some misalignment of the wing spar and follower axes.

The mechanism that creates the major flapping of the wings is a simple four-bar. The motor turns the two gear wheels (input crank), which in turn move the connecting rods (coupler) up and down. The connecting rods are pinned to the wing carriers, thus, rotating the wing carriers and wing spars (rocker) in a reciprocating manner about the flapping axis.

The mechanism that creates the feathering motion is a cam-follower system. It consists of a torsion spring, a bending spring, a follower, and a guide. The torsion spring is located near the center of the wing carrier between the two bearings that support the wing spar. The wing spar passes through the center of the torsion spring. One end of the torsion spring attaches to a small pin that extrudes from the wing spar, the other end attaches to the wing carrier. In this way, as the wing spar rotates relative to the wing carrier, the torsion spring is compressed and creates a moment about the wing spar axis. When the external force causing the rotation of the wing spar is removed, the torsion spring returns the wing spar to its original prontated position. Fig. 8 provides an illustration depicting the components of the wing carrier/torsion spring assembly.

The bending spring acts as a coupler connecting the follower to the wing spar. The bending spring allows for a slight misalignment of the follower while still transferring a moment from the follower to the wing spar. The bending spring has a second function of creating a moment that keeps the follower in contact with the guide. The bending spring is unstretched when the follower axis is in line with the wing spar axis.

The guide is a narrow ridge attached to the body of the ornithopter and positioned so that it lies in the path of the follower. A key feature of the guide is that its top edge is slightly in front of the follower axis and its bottom edge lies slightly behind the follower axis. The slight slant of the guide forces the follower to move along the back side of the guide, while moving downwards, and forced to move along the front side of the guide, while moving upwards.

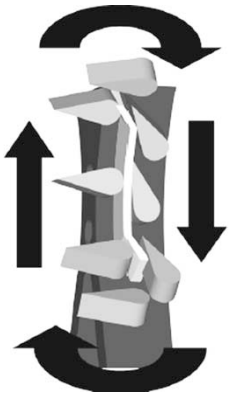

Fig. 9. Follower path around the guide. Because of the slant of the guide, the follower is forced to move along the backside of the guide while moving down and along the front side of the guide while moving up.

The follower motion is as follows: The follower begins slightly above the top edge of the guide. As the follower moves down, it contacts the guide. This contact occurs on the follower's flange forcing the follower to rotate about the feathering axis consequently rotating the entire wing. The follower then slides down the back edge of the guide with the torsion spring compressed. The bending spring forces the follower to remain in contact with the guide until the follower moves below the bottom edge of the guide. At this point, the bending spring and the torsion spring are released, rotating the wing to its original fully pronated position and realigning the follower axis with the wing spar axis. Next, the follower reverses directions and contacts the bottom edge of the guide. This time the follower is forced to move along the front edge of the guide, but with no flange on the backside of the follower the wing remains fully pronated. Fig. 9 illustrates the follower motion around the guide.

The actual prototype consists of a delrin body with integral delrin guides, nylon fabric wings attached to carbon fiber wing spars, a delrin follower attached to the wing spar by a small compression spring that acts as a bending spring, delrin connecting rods, a delrin wing carrier, nylon gear wheels, and a small DC motor. The only major difference between MHP II and MHP III is how the torsion spring is attached to the wing spar. MHP II attaches via a small pin in the wing spar through a hole drilled into the wing carrier. MHP III attaches via a hole in the wing carrier and a small hole in a hub attached to the wing spar. This connection has a drastic impact on the generated lift, as discussed later. The differences between the two attachments are shown in Fig. 10.

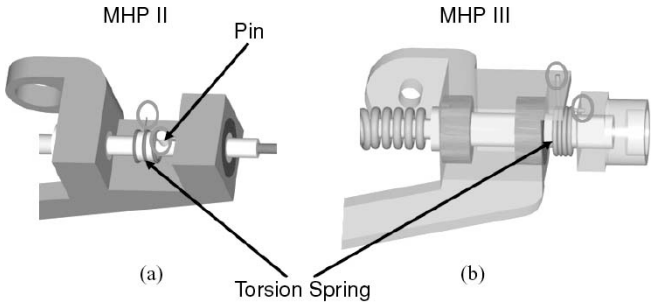

Fig. 10. (a) The torsion springs attachment points in MHP II. (b) The torsion springs attachment points for MHP III. Red circles indicate the attachment points for torsion springs.

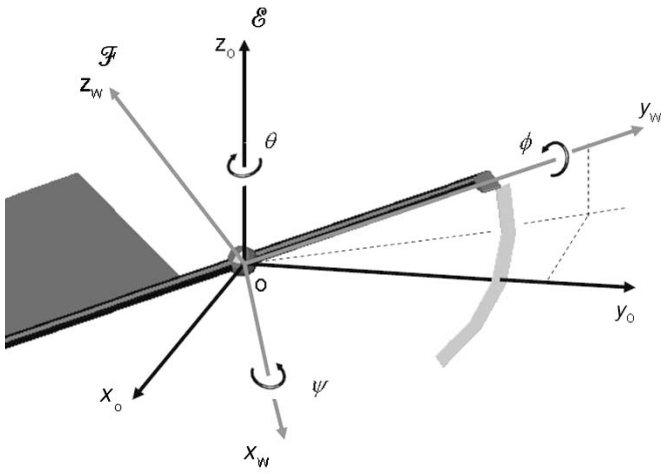

Fig. 11. Reference frame E is attached to the inertially fixed body and reference frame F is attached to the wing.

III. Dynamic Model of the Flapper Mechanism

The motivation of the dynamic model is to aid in determining the motion of the system and resulting external forces and moments on the wing. The most important information gained from the dynamic model is the aerodynamic lift and the power requirement of the device. An important goal of the mechanism is to generate enough lift to hover, while using a limited power source. The dynamic model provides the ability to see how changes in parameters affect the mechanism's performance and ultimately provides a tool to optimize the mechanism.

The theoretical model makes certain assumptions on the behavior of the physical model. In the theoretical model, the wing spar and follower are considered as one rigid link. This rigid link is considered to pivot about a spherical joint at the same position where the physical model pivots. The torsion spring in the theoretical model is applied in the same way as the physical model but the bending spring is modeled as a torsion spring about an axis perpendicular to the wing spar acting at the pivot point. In the theoretical model, the wing spar is allowed to rotate about three axes, as shown in Fig. 11. Rotation about the angle is assumed to be very small and friction is neglected due to the low-friction coefficient between the follower and the guide. Also, the transition period from the fully pronated position to the feathered position and vice versa is considered to be infinitesimally small. Finally, the body of the vehicle is assumed to be inertial fixed.

The reference frames of the mechanism are illustrated in Fig. 11. Reference frame E is inertially fixed and includes axes $x_{\mathrm{o}}, y_{\mathrm{o}}$, and z_{o} attached to the body of the ornithopter. Reference frame F rotates about E and includes axes $x_{\mathrm{w}}, y_{\mathrm{w}}$, and z_{w} attached to the wing. F is related to E by first a rotation about the z_{o}-axis, then a rotation Ψ about the new x-axis, and finally a rotation ϕ about

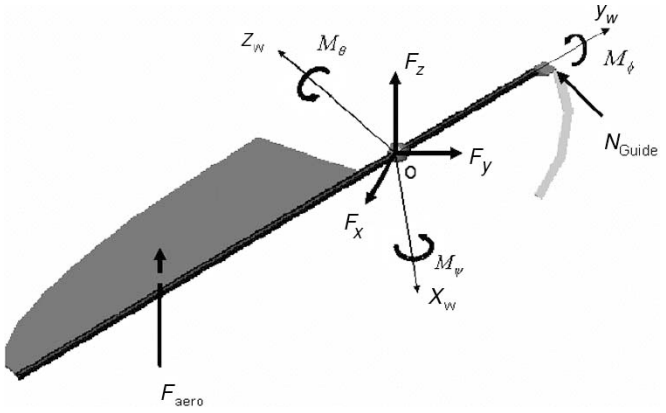

Fig. 12. Free body diagram shows the aerodynamic force, pivot support force, guide normal force, and the two spring moments that act on the wing.

the new y-axis (this is a body-sequence 3-1-2 rotation [12]). Both reference frames share the same origin at point o, the pivot point of the wing.

The forces and moments on the wing are shown in Fig. 12. The forces and moments include the following: 1) M_θ: this moment corresponds to the moment generated by the bending spring and is approximated as $M_\theta = -k_\theta \theta$. 2) M_ϕ: this moment corresponds to the moment generated by torsion spring and is approximated by $M_\phi = -k_\phi \phi$. 3) $\mathbf{F}_{\text{aero}}$: the aerodynamic force exerted on the wing as a function of wing position and angular speeds, as defined in [13] and discussed later in the paper. 4) M_Ψ: the input moment and corresponds to the force generated by the motor transmitted through the connecting rods. 5) $\mathbf{N}_{\text{guide}}$: the normal force exerted by the guide. 6) F_x, F_y, F_z: the reaction forces at the pivot support.

Because the wing pivots about the point o and the body of the ornithopter is considered inertially fixed in this analysis, only three orthogonal moment equations are necessary to completely define the motion of the wing. Also, because the unknown reaction forces F_x, F_y, and F_z do not create a moment about point o, these forces will not appear in the equations. The moment equations can be expressed in a matrix form as follows:

$$\mathbf{I} \cdot \tilde{\alpha} + \tilde{\omega} \times \mathbf{I} \cdot \tilde{\omega} = M \tag{1}$$

where $\tilde{\alpha}$ is the wing angular acceleration vector, $\tilde{\omega}$ is the wing angular velocity vector, and $\mathbf{I}$ is the wing inertia dyadic about o. M is the external moment vector about o and is the summation of all external moments. This vector equation can be expressed in F. The vector M in F is as follows:

$$M = R \begin{Bmatrix} M_\theta \\ M_\psi \\ M_\phi \end{Bmatrix} + TN + M_{\text{aero}} \tag{2}$$

where R is the matrix that transforms M_θ, M_ψ, and M_ϕ into F, and T is the matrix that transforms the normal force of the guide into a moment about point o in F. Here, N is the normal force generated by the guide. M_{aero} is the moment generated by the aerodynamic forces in F.

Using the property of the body-three rotation, ω is related to the time derivatives of the angles θ, ψ, and ϕ by

$$\begin{aligned} \omega_{x_{\text{w}}} &= \dot{\theta}\cos_\psi \sin_\phi - \dot{\psi}\cos_\phi \\ \omega_{y_{\text{w}}} &= \dot{\theta}\sin_\psi + \dot{\phi} \\ \omega_{z_{\text{w}}} &= \dot{\theta}\cos_\psi \cos_\phi + \dot{\alpha}\sin_\phi \end{aligned} \tag{3}$$

where $\omega_{x_{\text{w}}}, \omega_{y_{\text{w}}}$, and $\omega_{z_{\text{w}}}$ are the components of $\boldsymbol{w}$ in F, and cos and sin stand for cosine and sine. The expression for α is obtained by taking the time derivative of (3). Substituting these expressions in (1) and (2) and grouping like terms, the dynamic equations become:

$$\begin{aligned} A \begin{Bmatrix} \ddot{\theta} \\ \ddot{\psi} \\ \ddot{\phi} \end{Bmatrix} + B \begin{Bmatrix} \dot{\theta} \\ \dot{\psi} \\ \dot{\phi} \end{Bmatrix} + C \\ = D \begin{Bmatrix} M_\theta \\ M_\psi \\ M_\phi \end{Bmatrix} + EN + M_{\text{aero}} \end{aligned} \tag{4}$$

where A and B are (3×3) matrices and C is a (3×1) vector. D and E are (3×3) matrices to map the moments and forces in the equations of motion.

Since the slope of the guide is large, the rotation angle θ remains small. The connecting rod constrains only the angle ψ. If the speed of the motor is considered known, the motion of the connecting rods are known and consequently, $\psi, \dot{\psi}$, and $\ddot{\psi}$ are known. In (4), the unknowns are $\ddot{\theta}, \ddot{\phi}, M_\psi$, and N. With only three dynamic equations, a fourth constraint equation is necessary to solve the system of ODEs. This constraint is in terms of movement of the follower on the guide.

When the follower moves up on the front side of the guide, the normal force acts in a direction perpendicular to the guide. The moment generated by the bending spring constrains the follower to stay in contact with the guide. The equation of constraint is the equation of a line defined by the intersection of a sphere centered at the origin of radius l_{rod}, and a plane defined by the slope of the guide m passing through the origin. It can be written as follows:

$$m = \frac{z_1}{x_1} \tag{5}$$

where z_1 and x_1 are the coordinate positions of the tip of the wing spar and are functions of l_{rod} and the angles θ and ψ

$$\begin{aligned} x_1 &= -\sin(\theta)\cos(\psi) l_{\text{rod}} \\ z_1 &= \sin(\psi) l_{\text{rod}}. \end{aligned} \tag{6}$$

When the follower moves down the back side of the guide, the normal force again acts in a direction perpendicular to the guide, in this case though the normal force acts at the tip of the follower flange. This case can be written as follows:

$$m = \frac{z_2}{x_2} \tag{7}$$

where

$$\begin{aligned} x_2 &= (\cos_\theta \cos_\phi - \sin_\theta \sin_\alpha \sin_\phi) l_{\text{follower}} - \sin_\theta \cos_\alpha l_{\text{rod}} \\ z_2 &= -\cos_\alpha \sin_\phi l_{\text{follower}} + \sin_\alpha l_{\text{rod}}. \end{aligned} \tag{8}$$

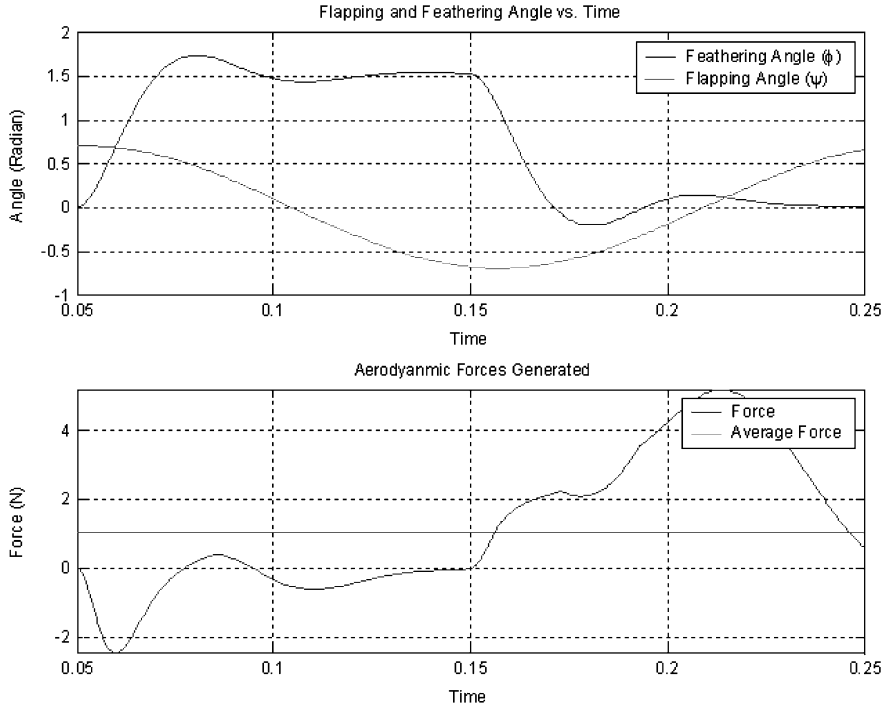

Fig. 13. Top graph shows the theoretical flap and feather angle. The bottom graph shows the predicted lift.

For the case when the follower is not in contact with the guide, at the very top and bottom of the stroke, the normal force is

$$N = 0. \tag{9}$$

For each case, the constraint equation takes the form

$$d_1\ddot{\theta} + d_2\ddot{\phi} + d_3 M_\alpha + d_4 N = d_5 \tag{10}$$

where the coefficients are functions of geometric and motion variables not involving $\ddot{\theta}, \ddot{\phi}, M_\psi$, and N. This constraint can be combined with the moment (4) in the following form:

$$H \begin{Bmatrix} \ddot{\theta} \\ \ddot{\phi} \\ M_\psi \\ N \end{Bmatrix} = \mathbf{J}, \tag{11}$$

Where all known quantities have been lumped in the (4×4) matrix H and vector $\mathbf{J}$. Finally, premultiplying (11) by H^{-1} gives a set of four coupled ODEs, which are solved using Matlab's ODE45 solver.

IV. Aerodynamic Model

The aerodynamic forces acting on the flapper are found using a model developed at the University of Delaware [13]. In the model, the wing is divided into n strips and the differential force resulting from each strip is computed. The expression for the differential force is given by

$$\Delta F = \frac{1}{2} C_1(\alpha_l)\rho \cdot c(r)\Delta r (V(d_i))^2 + C_3 \rho \frac{\pi}{4}(c(r))^2 \Delta r \cdot a. \tag{12}$$

This force has been shown to act normal to the wing surface at the specific cross section of the wing. In (12), ΔF is the differential force, ρ is the air density, r is distance from the wing base to the differential strip, $c(r)$ is the chord length at the corresponding length r, Δr is the thickness of the strip, $V(d_i)$ is the air velocity at a point on the wing strip 75% of the chord length, and α_l is the angle between the air velocity vector and the differential wing strip. The first term in the equation is an experimentally obtained model of the combined leading edge vortex (LEV) force and the rotational force [13]. The second term is the virtual mass effect. Because of the low wing mass, the virtual mass effect is considered negligible. A schematic of the aerodynamic model is shown in Fig. 12.

V. Theoretical Results

A computer program was developed using Matlab incorporating the above aerodynamic and dynamic model. The model uses the following parameters: The wing shape is a quarter ellipse with its minor axis measuring 0.14 m and major axis 0.30 m. The wing kinematics examines a flap rate from 1.2–1.9 Hz. The resulting lift generated by a flap rate of 1.5 Hz is shown in Fig. 13. The maximum lift is approximately 0.89 N and the average lift is 0.28 N. These flap rates are consistent with speeds of MHP II. Further theoretical data were obtained at 4 Hz, the flap rate of MHP III. Fig. 13 shows a graph of the aerodynamic force generated at 4 Hz.

There are two peaks during the upstroke and the downstroke seen in Fig. 13. The first negative peak occurs from rotational forces as the wing feathers before the upstroke. The second

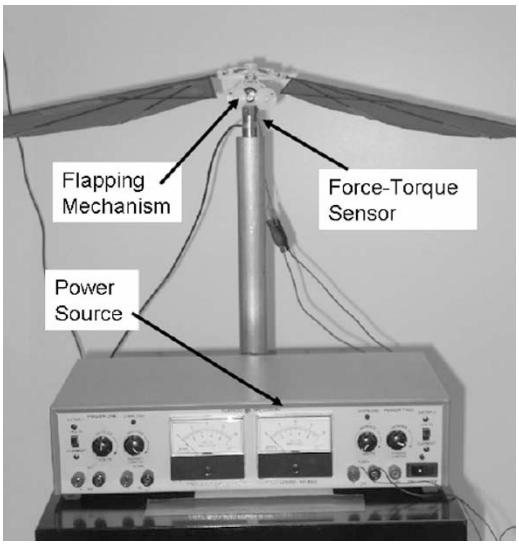

Fig. 14. Orithopter is mounted on a small force-torque sensor fixed on a rigid aluminum pedestal. The motor to drive the mechanism is powered by an Elenco power source.

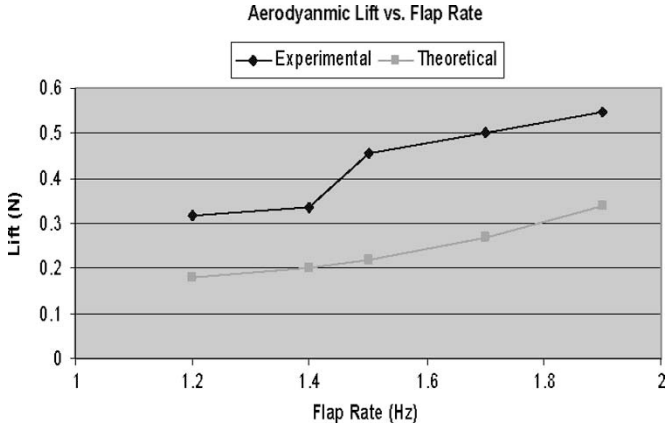

Fig. 15. Plot for the MHP II showing the average lift obtained experimentally and theoretically. The experimental values are larger than the theory but the shapes are similar.

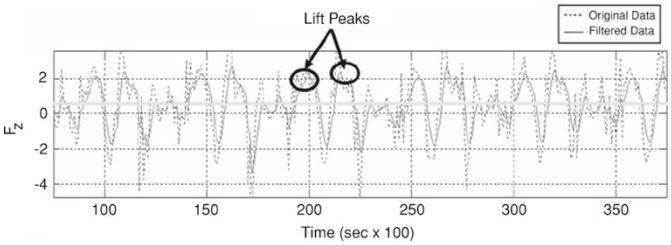

Fig. 16. Force sensor data of six complete flap cycles for MHP II is shown in the graphs. In each flap cycle, there are two major peaks that occur during the rapid wing twist at the top of the stroke and as the wing flaps downward. The flap rate is 1.9 Hz and the force measured in Newton.

negative peak is due to the translational forces during the upstroke. As the wing feathers prior to the downstroke there is a positive peak and a second larger peak as the wing translates during the downstroke. As hypothesized, the magnitude of lift during the downstroke is greater than the magnitude of negative lift during the upstroke, and consequently, there is a net lift.

VI. Experimental Results

In order to correlate with the theoretical results, a series of experiments were performed on MHP II to measure the actual force generated by the wings at various flap rates and the necessary power to run the mechanism. Similar experiments were run on MHP III. More accurate measurements of motor torques were made and an encoder was used to measure the flap angle.

The experimental setup consists of the mechanism mounted on a slender aluminum pedestal. In between the mechanism and the pedestal there is a small force-torque sensor, manufactured by ATI industrial automation. The data is collected using a dSPACE data acquisition board and is processed by a Matlab program. The mechanism's motor is powered by an Elenco Precision DC power source. The entire setup is shrouded in a large box to prevent interference from outside drafts. A photograph of the experimental setup is shown in Fig. 14. For the MHP III experiments, a small encoder from US digital was mounted to the main gear axle to measure the flap angle.

For the MHP II, the forces in x, y, and z were measured at six different voltage levels corresponding to five different flap rates. The most important force is of course the force in the z-direction, the lift. The average lift force for the six different flap rates and the corresponding voltages and currents was measured. Fig. 15 compares theses lifts to the theoretical predictions. Fig. 16 shows a graph of MHP II lift as a function of time at 1.9 Hz.

As predicted by the theoretical model, in the experimental data, as the flap rate increases so does the lift. Also, similar to the theoretical data, in the experimental data, there are two positive spikes followed by two smaller negative spikes in lift. For these experiments there was no measurement of wing position so it was not possible to see how the force data matches up with wing position. However, it shows similar trends in lift generation. Forces generated in the x and y directions were small compared to the z-direction. They were however sizable enough to potentially cause perturbations in the lateral motion of a flying prototype.

As mentioned earlier, the data collection for the MHP III experiments was more extensive. Fig. 17 shows a typical set of data collected for the MHP III. MHP III was able to flap its wings much faster than the MHP II. The MHP III could flap faster due mainly to improved quality of construction. Surprisingly, even with the increase in flap rate, MHP III did not generate nearly as much lift as MHP II. In fact, the majority of the forces generated with this prototype were in the x and y directions. A possible explanation for this is proposed later on.

The forces in the z-direction did follow a somewhat predicted pattern as seen in Fig. 18. During the downstroke, the lift generation was positive and during the upstroke the lift was negative. A possible explanation for this behavior lies in the feathering motion of the wing. As seen in Fig. 10, the torsion spring in MHP II is connected to the wing spar via a small pin. During the top of the upstroke, this pin prevented the wing from over rotation. This pin is not present in the MHP III design, consequently,

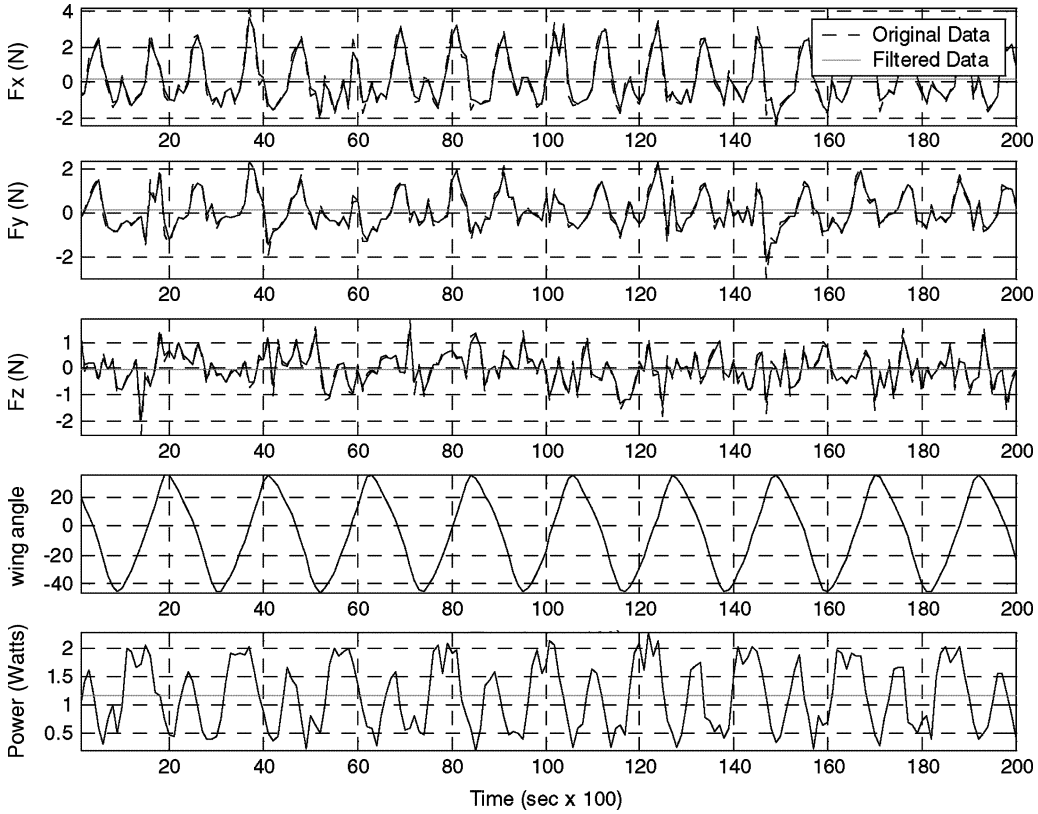

Fig. 17. Graphs show the F_x, F_y, and F_z forces along with the wing flap angle and power input.

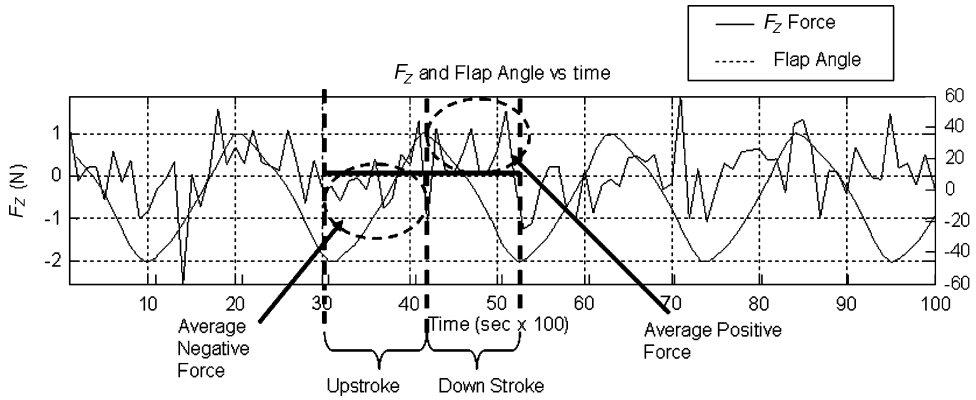

Fig. 18. Graph shows the force generation in the z-direction with respect to the flap angle of the wing.

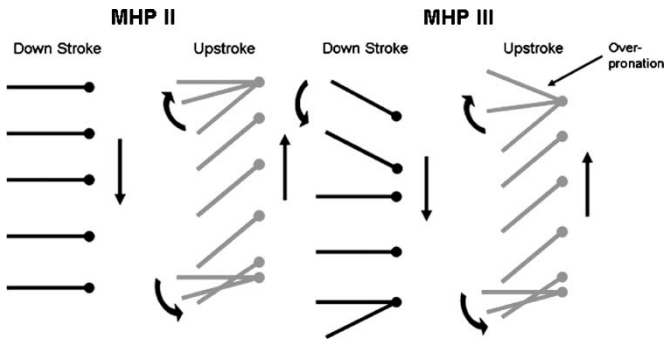

Fig. 19. First schematic shows the wing motion for MHP II. The second schematic shows the wing motion of MHP III.

the wing over pronates at the end of the upstroke reducing the wing's effective surface area during the downstroke. The wing motion of MHP II and MHP III is compared in Fig. 19.

VII. Conclusion

This paper presented a novel mechanism for biaxial rotation of an ornithopter wing, using a single actuator. This biaxial rotation was achieved by a spring-loaded cam-follower system, which was driven by a four-bar mechanism. The prototype demonstrates that hovering flight using biaxial wing rotation, generated by the proposed mechanism, is quite feasible. With instrumentation using force-torque sensors, it was demonstrated

that the experimental values of lift have similar trends with the theoretically predicted values and are in fact higher. This discrepancy is most likely due to neglecting the transition period between the fully pronated wing to the feathered wing, which causes the mismatch in the magnitude of lift. The present study is motivated from design of hovering vehicle and its dynamic characterization. Future work will address the issues of vehicle stability during free flight.

REFERENCES

[1] M. Grasmeyer and T. Keennon, "Development of the black widow micro air vehicle," *AIAA-2001-0127*.

[2] M. R. Waszak, J. B. Davidson, and P. G. Ifju, "Simulation and flight control of an aeroelastic fixed wing micro aerial vehicle," *AIAA 2002-4875*, presented at the *AIAA Atmospheric Flight Mechanics Conf.*, Monterey, CA, Aug., 2002.

[3] J. D. DeLaurier, "An aerodynamic model for flapping-wing flight," *Aeronaut. J.*, vol. 97, no. 964, pp. 125–130, Apr. 1993.

[4] T. Pornsin-Sirirak, S. Lee, H. Nassif, J. Grasmeyer, Y. Tai, C. Ho, and M. Keennon, "MEMS wing technology for a battery-powered ornithopter," in *Proc. 13th IEEE Int. Conf. MEMS*, Miyazaki, Japan, Jan. 2000, pp. 799–804.

[5] R. J. Wood, S. Avadhanula, and R. S. Fearing, "Microrobotics using composite materials: The micromechanical flying insect thorax," in *IEEE Int. Conf. Robotics and Autoation*, Taipei, Taiwan, 2003, pp. 1842–1849.

[6] C. P. Ellington, "The aerodynamics of hovering insect flight," *Philos. Trans. Roy. Soc. London*, Series B, vol. 305, pp. 1–15, 1984.

[7] S. P. Sane and M. H. Dickinson, "The aerodynamic effects of wing rotation and a revised quasi-steady model of flapping flight," *J. Exp. Biol.*, vol. 205, pp. 1087–1096, 2002.

[8] Z. A. Khan and S. K. Agrawal, "Wing force and moment characterization of flapping wings for micro air vehicle application," presented at the *Amer. Control Conf.*, Orlando, FL, 2005.

[9] R. Madangopal, Z. Khan, and S. K. Agrawal, "Biologically inspired design of small flapping wing air vehicles using four bar mechanisms and quasi-steady aerodynamics," *J. Mech. Design Trans. ASME*, vol. 127, pp. 809–816, 2005.

[10] S. Banala and S. K. Agrawal, "Design and optimization of a mechanism for out of plane insect wing like motion with twist," *J. Mech. Design Trans. ASME*, vol. 127, pp. 841–844, 2005.

[11] M. McDonald, "Design of flapping-wing micro-aerial vehicles motivated by hawk moths and hummingbirds," Undergraduate Thesis.Univ. Delaware, Newark, 2005.

[12] T. Kane, P. Linkins, and D. Levinson, *Spacecraft Dynamics*. New York: McGraw-Hill, 1983.

Sean H. McIntosh (M'76–SM'81–F'87) was born in Nuremberg, Germany, on November 14, 1981.He received the B.S. and M.S. degrees from the University of Delaware, Newark, DE, in 2003 and 2006, respectively, both in mechanical engineering.

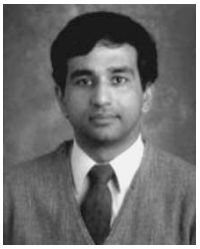

Sunil K. Agrawal (M'92) received the Ph.D. degree in mechanical engineering from the Stanford University, Stanford, CA, in 1990.

He has worked in universities, government laboratories, and industries around the world. He is a Professor of mechanical engineering at the University of Delaware, Newark. His research has made contributions in robotics and control, including novel designs of robots and autonomous systems, computational algorithms for planning and optimization of dynamic systems, and devices for medical rehabilitation. His work has yielded over 225 technical publications and two books.

Dr. Agrawal is a fellow of ASME, since 2004. He was the recipient of a National Science Foundation (NSF) Presidential Faculty Fellowship from the White House and a Freidrich Wilheim Bessel prize from Alexander von Humboldt Foundation, Germany.

Zaeem Khan was born in Karachi, Pakistan, on September 11, 1973. He received the B.E. degree in mechanical engineering from the NED University of Engineering and Technology, Karachi, Pakistan, in 1998, and the M.S. degree in mechanical engineering from the University of Delaware, Newark, in 2005. He is currently pursuing the Ph.D. degree in biomechanics and movement science program.

From 1999 to 2001, he worked in the automobile industry as a CAD/CAM Engineer. Currently, he is with the University of Delaware, Newark. The major area of research is the study of biomechanics of insect flight with application to flapping wing micro air vehicle design and development.

Dr. Khan is a member of ASME. He has been the recepient of the Employee of the Year Award for 1999.